Nonlinear Control of a Dual-Quadrotor Assembly

Anthony Dzaba and Eugenio Schuster

***Abstract*—In response to the need for accurate position sensing in unmanned aerial vehicles (UAVs), we propose a concept aircraft in the form of a mobile global vision system. The dual-quad prototype resembles a miniature quadrotor nesting within a larger quadrotor. Inspired by the gaze stabilization abilities of hunting birds, the inner quadrotor is used as an actively stabilized sensor deck, while the outer quadrotor is used as a position-control flight deck. The sensor deck is stabilized to impose motion constraints on the visual odometry problem. This reduces the computational expense of implementing a vision system on a UAV where resources are limited. We propose a combination of feedback linearization, nonlinear transformation, and backstepping control. Results for aggressive flight maneuvers are demonstrated in simulation.**

I. Introduction

Advanced motion control techniques capable of producing aggressive flight maneuvers, generally require non-portable, high-precision pose measurement systems such as the Vicon camera array used to track the agile micro quadrotors featured in [1]. In order to duplicate these results outside of the laboratory setting, one would be faced with the difficult task of integrating capable on-board vision systems on micro aerial vehicles (MAVs) where resources are at a premium. For this reason it may prove more expedient to avoid giving each MAV "eyes" and instead give a single global vision system "wings". To this end we envision a mobile global vision system. The concept of a dedicated airborne tracking asset becomes familiar when we consider the airborne warning and control system (AWACS). To reduce the computational expense of implementing vision-based tracking on a UAV-size AWACS, we look to introduce motion constraints. Specifically, fixing the rotation of the vision system (with respect to the scene under observation) reduces the visual odometry problem to a simpler 3D correlation task.

We borrow from a familiar biological solution in which a bird of prey is able to isolate the chaotic motion of its body (flight frame) from the stabilized motion of its head (sensor frame), which continuously tracks a target of interest [2]. This type of attitude decoupling would prove difficult should our AWACS UAV assume the form of a quadrotor, which by reason of underactuation, must change its attitude in order to change its position. We address this issue by designing a novel aircraft featuring an additional set of actuators in the form of a second nested quadrotor (increasing the system's degrees of freedom from six to nine). The ramifications of this design choice are discussed in the Conclusions section.

From the vast body of work dedicated to quadrotor backstepping, we site the following examples. A classical three-step backstepping controller is proposed in [3]. A simplified backstepping approach with a nested saturation controller is proposed in [4]. A combination of backstepping and adaptive sliding mode control is proposed in [5]. A combination of backstepping and robust control, designed to address model parameter uncertainty, is proposed in [6]. Lastly, a Lagrange-form backstepping controller with neural network estimation of the attitude dynamics is proposed in [7].

In this paper, we propose a combination of feedback linearization, nonlinear transformation, and backstepping control to stabilize the seven outputs, which are the 3D sensor deck attitude, the scalar flight deck yaw heading, and the 3D position. We begin by simplifying the dynamics of the sensor deck and flight deck attitude states using feedback linearization. Next, we use PD controllers to stabilize the altitude and flight deck yaw heading. Next, we decouple the horizontal position states using a nonlinear transformation. And last, we stabilize the horizontal position via the flight deck's pitch and roll states using a backstepping controller.

This paper is organized as follows. In Section II, we derive the equations of motion for the dual-quad using the Euler-Lagrange equation. In Section III, we develop the backstepping framework. In Section IV, we present Simulation results. Finally, in Section V, we discuss conclusions, design considerations, and future work.

II. Equations of Motion

The dual-quad is actuated by eight brushless DC motors outfitted with orthogonal sets of counter-rotating propellers. The outer quadrotor is designated as the flight deck while the inner quadrotor is designated as the sensor deck. The two decks are connected via a ball joint assembly, as illustrated in Fig. 1. The equations of motion are derived in the inertial frame using the approach proposed in [4]. The inertial axes are separated from the Earth-fixed axes by a 3D translation vector and a scalar yaw rotation denoted ψ_f. The dual-quad position is given by the 3D vector $\xi = [x, y, z]^T$. The dual-quad attitude is defined by two sets of body-fixed axes. The attitude of the flight deck is given by the Tait-Bryan angles $\eta_f = [\psi_f, \theta_f, \phi_f]^T$, while the attitude of the sensor deck is given by the analogous angles $\eta_s = [\psi_s, \theta_s, \phi_s]^T$. The model assumes perfect knowledge of the states.

With $q = [\xi, \eta_f, \eta_s]^T$, we define the Lagrangian

$$L(q, \dot{q}) = T_{trans} + T_{rot} + U, \tag{1}$$

$$T_{trans} = \frac{m}{2}\dot{\xi}^T\dot{\xi},\ T_{rot} = \frac{1}{2}\Omega_f^T\mathbf{I}_f\Omega_f + \frac{1}{2}\Omega_s^T\mathbf{I}_s\Omega_s, \tag{2}$$

$$U = -mgz,\ \Omega_f = W_v(\eta_f)\dot{\eta}_f,\ \Omega_s = W_v(\eta_s)\dot{\eta}_s, \tag{3}$$

A. Dzaba (anthony@lehigh.edu) and E. Schuster are with the Department of Mechanical Engineering, Lehigh University, Bethlehem, PA 18015 USA.

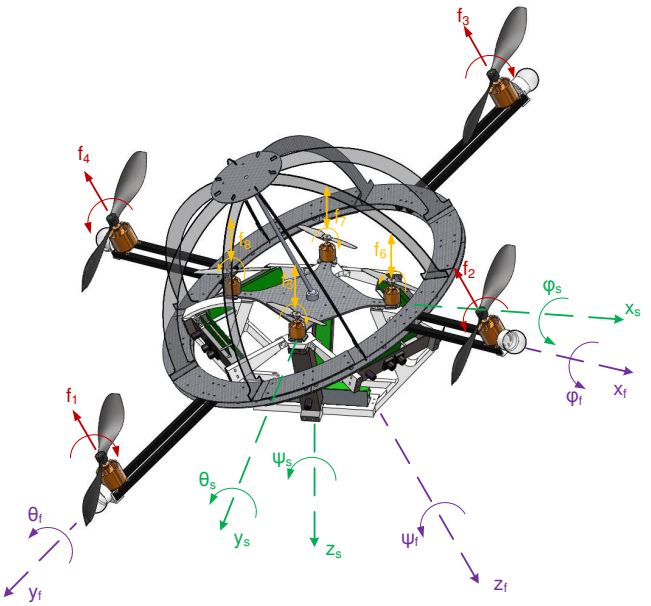

Figure 1. By design, the orientation of the flight deck (purple axes) is independent of the orientation of the sensor deck (green axes). The two decks are connected via the stem which originates at the anterior apex of the dome and terminates at the ball joint in the center of the sensor deck.

$$W_v(\eta) = \begin{bmatrix} -\sin\theta & 0 & 1 \\ \cos\theta\sin\psi & \cos\psi & 0 \\ \cos\theta\cos\psi & -\sin\psi & 0 \end{bmatrix}, \tag{4}$$

where $\mathbf{I}_f$ and $\mathbf{I}_s$ are the moment of inertia tensors for the flight deck and sensor deck, respectively, m is the vehicle mass, and g is the acceleration due to gravity. The vectors Ω_f and Ω_s are the 3D angular velocities of the flight deck and the sensor deck in their respective frames.

In the vehicle-fixed frames, the external forces are

$$F_f = \begin{bmatrix} 0 \\ 0 \\ -F_{f_z} \end{bmatrix} \triangleq \begin{bmatrix} 0 \\ 0 \\ (f_3+f_1)+(f_2+f_4) \end{bmatrix}, \tag{5}$$

$$F_s = \begin{bmatrix} 0 \\ 0 \\ F_{s_z} \end{bmatrix} \triangleq \begin{bmatrix} 0 \\ 0 \\ (f_7+f_5)+(f_6+f_8) \end{bmatrix}, \tag{6}$$

$$\tau_f = \begin{bmatrix} \tau_{f_\psi} \\ \tau_{f_\theta} \\ \tau_{f_\phi} \end{bmatrix} \triangleq \begin{bmatrix} (f_3+f_1)b_f-(f_2+f_4)b_f \\ (f_2-f_4)l_f \\ (f_3-f_1)l_f \end{bmatrix}, \tag{7}$$

$$\tau_s = \begin{bmatrix} \tau_{s_\psi} \\ \tau_{s_\theta} \\ \tau_{s_\phi} \end{bmatrix} \triangleq \begin{bmatrix} (f_7+f_5)b_s-(f_6+f_8)b_s \\ (f_6-f_8)l_s \\ (f_7-f_5)l_s \end{bmatrix}, \tag{8}$$

where F_f and F_s are the cumulative thrusts, and τ_f and τ_s are the 3D moments on the flight deck and sensor deck, respectively. The scalars $f_{i=1:4} \in \begin{bmatrix} 0 & f_{f_{max}} \end{bmatrix}$ are the four (non-negative) flight deck rotor thrusts, and $f_{i=5:8} \in \begin{bmatrix} -f_{s_{max}} & f_{s_{max}} \end{bmatrix}$ are the four sensor deck rotor thrusts. The parameters b_f and b_s are positive electromechanical constants, and l_f and l_s are the moment arms between opposing motors on the flight and sensor decks, respectively. Note that the sums and differences on the right-hand side of (5)-(8) are eight independent equations in the eight inputs.

We map F_f and F_s to the inertial frame using

$$F_\xi = R(\eta_f)F_f + R(\eta_s)F_s, \tag{9}$$

$$R(\eta) = \begin{bmatrix} c_\psi c_\theta & c_\theta s_\psi & -s_\theta \\ c_\psi s_\theta s_\phi - c_\phi s_\psi & c_\psi c_\phi + s_\psi s_\theta s_\phi & c_\theta s_\phi \\ s_\psi s_\phi + c_\psi c_\phi s_\theta & c_\phi s_\psi s_\theta - c_\psi s_\phi & c_\phi c_\theta \end{bmatrix}, \tag{10}$$

where R is the rotation matrix from the flight or sensor frame to the inertial frame. The functions $\sin\theta$ and $\cos\phi$ have been abbreviated as s_θ and c_ϕ. Evaluating the Lagrangian,

$$\frac{d}{dt}\frac{\partial \mathcal{L}}{\partial \dot{q}} - \frac{\partial \mathcal{L}}{\partial q} = \begin{bmatrix} F_\xi & \tau_f & \tau_s \end{bmatrix}^T, \tag{11}$$

we obtain the equations of motion

$$m\ddot{\xi} + \begin{bmatrix} 0 \\ 0 \\ -mg \end{bmatrix} = R(\eta_f)F_f + R(\eta_s)F_s, \tag{12}$$

$$\mathbb{J}(\eta_f, \mathbf{I}_f)\ddot{\eta}_f + C(\eta_f, \dot{\eta}_f)\dot{\eta}_f = \tau_f, \tag{13}$$

$$\mathbb{J}(\eta_s, \mathbf{I}_s)\ddot{\eta}_s + C(\eta_s, \dot{\eta}_s)\dot{\eta}_s = \tau_s, \tag{14}$$

$$\mathbb{J}(\eta, \mathbf{I}) = W_v^T(\eta)\mathbf{I}W_v(\eta), \tag{15}$$

$$C(\eta, \dot{\eta}) = \dot{\mathbb{J}} - \frac{1}{2}\frac{\partial}{\partial \eta}(\dot{\eta}^T\mathbb{J}), \tag{16}$$

$$\begin{bmatrix} \ddot{x} \\ \ddot{y} \\ \ddot{z} \end{bmatrix} = \frac{1}{m}\begin{bmatrix} -F_{f_z}s_{\theta_f} - F_{s_z}s_{\theta_s} \\ F_{f_z}c_{\theta_f}s_{\phi_f} + F_{s_z}c_{\theta_s}s_{\phi_s} \\ -F_{f_z}c_{\theta_f}c_{\phi_f} - F_{s_z}c_{\theta_s}c_{\phi_s} + mg \end{bmatrix}, \tag{17}$$

$$\begin{bmatrix} \ddot{\psi}_f \\ \ddot{\theta}_f \\ \ddot{\phi}_f \end{bmatrix} = \mathbb{J}^{-1}(\eta_f, \mathbf{I}_f)\left(\begin{bmatrix} \tau_{f_\psi} \\ \tau_{f_\theta} \\ \tau_{f_\phi} \end{bmatrix} - C(\eta_f, \dot{\eta}_f)\begin{bmatrix} \dot{\psi}_f \\ \dot{\theta}_f \\ \dot{\phi}_f \end{bmatrix}\right), \tag{18}$$

$$\begin{bmatrix} \ddot{\psi}_s \\ \ddot{\theta}_s \\ \ddot{\phi}_s \end{bmatrix} = \mathbb{J}^{-1}(\eta_s, \mathbf{I}_s)\left(\begin{bmatrix} \tau_{s_\psi} \\ \tau_{s_\theta} \\ \tau_{s_\phi} \end{bmatrix} - C(\eta_s, \dot{\eta}_s)\begin{bmatrix} \dot{\psi}_s \\ \dot{\theta}_s \\ \dot{\phi}_s \end{bmatrix}\right), \tag{19}$$

with inputs $F_{f_z} \in R$, $F_{s_z} \in R$, $\tau_f \in R^3$, and $\tau_s \in R^3$.

III. Control Scheme

In Section III-A, we simplify the system dynamics via feedback. In Section III-B, we use a set of PD controllers to stabilize the sensor deck attitude. In Section III-C we use a similar set of controllers to stabilize the vehicle altitude and the flight deck yaw heading. In Section III-D, we present a backstepping control strategy for stabilizing the horizontal position using the flight deck pitch and roll states. A block diagram of the control system is given in Fig. 2. The top two rows show the feedback linearization control of z and ψ_f. The bottom row illustrates the combined state feedback and backstepping control processes for the x and y states.

A. Feedback Linearization

First, we simplify the dynamics of the six attitude states by substituting the feedback linearization control laws

$$\tau_f \triangleq C(\eta_f, \dot{\eta}_f)\dot{\eta}_f + \mathbb{J}_f(\eta_f)\begin{bmatrix} r_{\psi_f} & r_{\theta_f} & r_{\phi_f} \end{bmatrix}^T, \tag{20}$$

$$\tau_s \triangleq C(\eta_s, \dot{\eta}_s)\dot{\eta}_s + \mathbb{J}_s(\eta_s)\begin{bmatrix} r_{\psi_s} & r_{\theta_s} & r_{\phi_s} \end{bmatrix}^T, \tag{21}$$

into (18) and (19) to obtain the linear subsystems

$$\begin{bmatrix} \ddot{\psi}_f & \ddot{\theta}_f & \ddot{\phi}_f \end{bmatrix}^T = \begin{bmatrix} r_{\psi_f} & r_{\theta_f} & r_{\phi_f} \end{bmatrix}^T, \tag{22}$$

$$\begin{bmatrix} \ddot{\psi}_s & \ddot{\theta}_s & \ddot{\phi}_s \end{bmatrix}^T = \begin{bmatrix} r_{\psi_s} & r_{\theta_s} & r_{\phi_s} \end{bmatrix}^T, \tag{23}$$

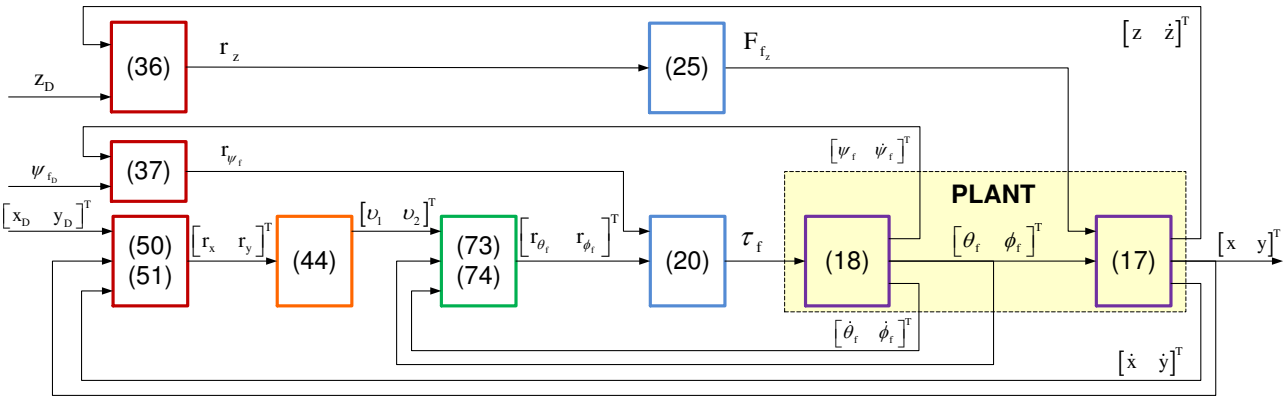

Figure 2. Each block in the diagram represents an equation in the text. The control design linearizes the system from the references $\begin{bmatrix} x_D & y_D & z_D & \psi_{f_D} \end{bmatrix}^T$, to the outputs $\begin{bmatrix} x & y & z & \psi_f \end{bmatrix}^T$. Note that the decoupled states z and ψ_f (as well as the sensor deck states ψ_s, θ_s, and ϕ_s, not pictured) are controlled outside of the backstepping framework.

where r_{ψ_f}, r_{θ_f}, and r_{ϕ_f} are the new control inputs to the flight deck subsystem, and r_{ψ_s}, r_{θ_s}, and r_{ϕ_s} are the new control inputs to the sensor deck subsystem. Next, we decouple the forces on the sensor deck from those of the attitude deck by setting $F_{s_z} \triangleq 0$, so that (17) simplifies to

$$\begin{bmatrix} \ddot{x} \\ \ddot{y} \\ \ddot{z} \end{bmatrix} = \frac{1}{m} \begin{bmatrix} -F_{f_z} s_{\theta_f} \\ F_{f_z} c_{\theta_f} s_{\phi_f} \\ -F_{f_z} c_{\theta_f} c_{\phi_f} + mg \end{bmatrix}. \tag{24}$$

We then use the feedback linearization control law

$$F_{f_z} \triangleq m \frac{r_z + g}{\cos\theta_f \cos\phi_f}, \tag{25}$$

to simplify the altitude state in (24), which becomes

$$\begin{bmatrix} \ddot{x} \\ \ddot{y} \\ \ddot{z} \end{bmatrix} = \begin{bmatrix} -(r_z + g)\sec\phi_f \tan\theta_f \\ (r_z + g)\tan\phi_f \\ -r_z \end{bmatrix}, \tag{26}$$

where the position control inputs are now θ_f, ϕ_f, and r_z.

B. Stabilization of the Sensor Deck Attitude

First, we convert the second-order system (23), into the equivalent first-order system

$$\gamma = \begin{bmatrix} \gamma_1 \\ \gamma_2 \\ \gamma_3 \\ \gamma_4 \\ \gamma_5 \\ \gamma_6 \end{bmatrix} = \begin{bmatrix} \psi_s \\ \theta_s \\ \phi_s \\ \dot{\psi}_s \\ \dot{\theta}_s \\ \dot{\phi}_s \end{bmatrix}, \begin{bmatrix} \dot{\gamma}_1 \\ \dot{\gamma}_2 \\ \dot{\gamma}_3 \\ \dot{\gamma}_4 \\ \dot{\gamma}_5 \\ \dot{\gamma}_6 \end{bmatrix} = \begin{bmatrix} \gamma_4 \\ \gamma_5 \\ \gamma_6 \\ r_{\psi_s} \\ r_{\theta_s} \\ r_{\phi_s} \end{bmatrix}, \tag{27}$$

where r_{ψ_f}, r_{θ_f}, and r_{ϕ_f} are the inputs, and γ_1, γ_2, and γ_3, are the outputs. We define the control laws

$$r_{\psi_s} \triangleq -2k_{\gamma_1}\gamma_4 - k_{\gamma_1}^2\gamma_1, \tag{28}$$
$$r_{\theta_s} \triangleq -2k_{\gamma_2}\gamma_5 - k_{\gamma_2}^2\gamma_2, \tag{29}$$
$$r_{\phi_s} \triangleq -2k_{\gamma_3}\gamma_6 - k_{\gamma_3}^2\gamma_3, \tag{30}$$

where k_{γ_1}, k_{γ_2}, and k_{γ_3} are the positive-definite control gains. Substituting (28)-(30) into (27), we find the linear subsystems

$$\begin{bmatrix} \dot{\gamma}_1 \\ \dot{\gamma}_3 \end{bmatrix} = A_{\gamma_1} \begin{bmatrix} \gamma_1 \\ \gamma_4 \end{bmatrix}, A_{\gamma_1} = \begin{bmatrix} 0 & 1 \\ -k_{\gamma_1}^2 & -2k_{\gamma_1} \end{bmatrix}, \tag{31}$$
$$\begin{bmatrix} \dot{\gamma}_2 \\ \dot{\gamma}_4 \end{bmatrix} = A_{\gamma_2} \begin{bmatrix} \gamma_2 \\ \gamma_5 \end{bmatrix}, A_{\gamma_2} = \begin{bmatrix} 0 & 1 \\ -k_{\gamma_2}^2 & -2k_{\gamma_2} \end{bmatrix}, \tag{32}$$
$$\begin{bmatrix} \dot{\gamma}_3 \\ \dot{\gamma}_6 \end{bmatrix} = A_{\gamma_3} \begin{bmatrix} \gamma_3 \\ \gamma_6 \end{bmatrix}, A_{\gamma_3} = \begin{bmatrix} 0 & 1 \\ -k_{\gamma_3}^2 & -2k_{\gamma_3} \end{bmatrix}, \tag{33}$$

where $\text{eig}(A_{\gamma_i}) = \begin{bmatrix} -k_{\gamma_i} & -k_{\gamma_i} \end{bmatrix}^T, \forall i = 1:3$, making the closed-loop γ-subsystem globally, exponentially stable.

C. Stabilization of the Flight Deck Altitude and Yaw

By stabilizing the error signals

$$\begin{bmatrix} z_e(t) \\ \psi_e(t) \\ \dot{z}_e(t) \\ \dot{\psi}_e(t) \end{bmatrix} = \begin{bmatrix} z(t) - z_D(t) \\ \psi(t) - \psi_{f_D}(t) \\ \dot{z}(t) - \dot{z}_D(t) \\ \dot{\psi}(t) - \dot{\psi}_{f_D}(t) \end{bmatrix}, \tag{34}$$

we can track the altitude reference, $z_D(t)$, and the yaw reference, $\psi_{f_D}(t)$. As before, we first convert the second-order systems (22) and (26), into the first-order system

$$\alpha = \begin{bmatrix} \alpha_1 \\ \alpha_2 \\ \alpha_3 \\ \alpha_4 \end{bmatrix} = \begin{bmatrix} z_e \\ \psi_{f_e} \\ \dot{z}_e \\ \dot{\psi}_{f_e} \end{bmatrix}, \begin{bmatrix} \dot{\alpha}_1 \\ \dot{\alpha}_2 \\ \dot{\alpha}_3 \\ \dot{\alpha}_4 \end{bmatrix} = \begin{bmatrix} \alpha_3 \\ \alpha_4 \\ -r_z - \ddot{z}_D(t) \\ r_{\psi_f} - \ddot{\psi}_{f_D}(t) \end{bmatrix}, \tag{35}$$

where r_z and r_{ψ_f} are the inputs, and α_1 and α_2 are the outputs. We define the control laws

$$-r_z \triangleq -2k_{\alpha_1}\alpha_3 - k_{\alpha_1}^2\alpha_1 + \ddot{z}_D(t), \tag{36}$$
$$r_{\psi_f} \triangleq -2k_{\alpha_2}\alpha_4 - k_{\alpha_2}^2\alpha_2 + \ddot{\psi}_{f_D}(t), \tag{37}$$

where k_{α_1} and k_{α_2} are the positive-definite control gains. Substituting (36) and (37) into (35), we obtain the globally, exponentially stable subsystems

$$\begin{bmatrix} \dot{\alpha}_1 \\ \dot{\alpha}_3 \end{bmatrix} = A_{\alpha_1} \begin{bmatrix} \alpha_1 \\ \alpha_3 \end{bmatrix}, A_{\alpha_1} = \begin{bmatrix} 0 & 1 \\ -k_{\alpha_1}^2 & -2k_{\alpha_1} \end{bmatrix}, \tag{38}$$
$$\begin{bmatrix} \dot{\alpha}_2 \\ \dot{\alpha}_4 \end{bmatrix} = A_{\alpha_2} \begin{bmatrix} \alpha_2 \\ \alpha_4 \end{bmatrix}, A_{\alpha_2} = \begin{bmatrix} 0 & 1 \\ -k_{\alpha_2}^2 & -2k_{\alpha_2} \end{bmatrix}. \tag{39}$$

D. Stabilization of the Flight Deck Horizontal Position

By stabilizing the error signals

$$\begin{bmatrix} x_e(t) \\ y_e(t) \end{bmatrix} = \begin{bmatrix} x(t) - x_D(t) \\ y(t) - y_D(t) \end{bmatrix}, \tag{40}$$

we can track the position references $x_D(t)$ and $y_D(t)$. We begin by converting (22) and (26) into the equivalent system

$$\beta = \begin{bmatrix} \beta_1 \\ \beta_2 \\ \beta_3 \\ \beta_4 \end{bmatrix} = \begin{bmatrix} x_e \\ y_e \\ \dot{x}_e \\ \dot{y}_e \end{bmatrix}, \ \delta = \begin{bmatrix} \delta_1 \\ \delta_2 \\ \delta_3 \\ \delta_4 \end{bmatrix} = \begin{bmatrix} \theta_f \\ \phi_f \\ \dot{\theta}_f \\ \dot{\phi}_f \end{bmatrix}, \tag{41}$$

$$\begin{bmatrix} \dot{\beta}_1 \\ \dot{\beta}_2 \\ \dot{\beta}_3 \\ \dot{\beta}_4 \end{bmatrix} = \begin{bmatrix} \beta_3 \\ \beta_4 \\ -(r_z + g)\sec\delta_2 \tan\delta_1 - \ddot{x}_D(t) \\ (r_z + g)\tan\delta_2 - \ddot{y}_D(t) \end{bmatrix}, \tag{42}$$

$$\begin{bmatrix} \dot{\delta}_1 & \dot{\delta}_2 & \dot{\delta}_3 & \dot{\delta}_4 \end{bmatrix}^T = \begin{bmatrix} \delta_3 & \delta_4 & r_{\theta_f} & r_{\phi_f} \end{bmatrix}^T, \tag{43}$$

with inputs r_{θ_f} and r_{ϕ_f}, and outputs β_1 and β_2.

Using the nonlinear transformation

$$\upsilon = \begin{bmatrix} \upsilon_1 \\ \upsilon_2 \\ \upsilon_3 \\ \upsilon_4 \end{bmatrix} \triangleq \begin{bmatrix} -\sec\delta_2 \tan\delta_1 - \frac{r_x}{r_z+g} \\ \tan\delta_2 - \frac{r_y}{r_z+g} \\ \dot{\upsilon}_1 \\ \dot{\upsilon}_2 \end{bmatrix}, \tag{44}$$

we convert the β-δ system (42)-(43), to the β-υ system

$$\begin{bmatrix} \dot{\beta}_1 \\ \dot{\beta}_3 \end{bmatrix} = \begin{bmatrix} \beta_3 \\ -(r_z + g)\upsilon_1 + r_x - \ddot{x}_D(t) \end{bmatrix}, \begin{bmatrix} \dot{\upsilon}_1 \\ \dot{\upsilon}_3 \end{bmatrix} = \begin{bmatrix} \upsilon_3 \\ \mu_1 \end{bmatrix}, \tag{45}$$

$$\begin{bmatrix} \dot{\beta}_2 \\ \dot{\beta}_4 \end{bmatrix} = \begin{bmatrix} \beta_4 \\ (r_z + g)\upsilon_2 + r_y - \ddot{y}_D(t) \end{bmatrix}, \begin{bmatrix} \dot{\upsilon}_2 \\ \dot{\upsilon}_4 \end{bmatrix} = \begin{bmatrix} \upsilon_4 \\ \mu_2 \end{bmatrix}, \tag{46}$$

$$\begin{aligned} \mu_1 \triangleq\ & (\cos^2\delta_2(2\sin\delta_1\delta_3^2 - \sin\delta_1\delta_4^2\cos^2\delta_1 + r_{\theta_f}\cos\delta_1) \\ & + \cos\delta_2(r_{\phi_f}\sin\delta_1\sin\delta_2\cos^2\delta_1 + 2\delta_3\delta_4\sin\delta_2\cos\delta_1) \\ & + 2\delta_4^2\cos^2\delta_1\sin\delta_1)\sec^3\delta_1\sec^3\delta_2 \\ & - \frac{d^2}{dt^2}\left(\frac{2k_{\beta_1}\beta_3 + k_{\beta_1}^2\beta_1 - \ddot{x}_D(t)}{r_z + g}\right), \end{aligned} \tag{47}$$

$$\begin{aligned} \mu_2 \triangleq\ & \sec^2\delta_2(2\delta_4^2\tan\delta_2 + r_{\phi_f}) \\ & - \frac{d^2}{dt^2}\left(\frac{-2k_{\beta_2}\beta_4 - k_{\beta_2}^2\beta_2 + \ddot{y}_D(t)}{r_z + g}\right), \end{aligned} \tag{48}$$

$$\begin{bmatrix} \delta_1 \\ \delta_2 \end{bmatrix} = \begin{bmatrix} -\arctan\left(\left(\upsilon_1 + \frac{r_x}{r_z+g}\right)\cos\delta_2\right) \\ \arctan\left(\upsilon_2 + \frac{r_y}{r_z+g}\right) \end{bmatrix}, \tag{49}$$

$$r_x \triangleq -2k_{\beta_1}\beta_3 - k_{\beta_1}^2\beta_1 + \ddot{x}_D(t)\ , \tag{50}$$

$$r_y \triangleq -2k_{\beta_2}\beta_4 - k_{\beta_2}^2\beta_2 + \ddot{y}_D(t)\ , \tag{51}$$

where k_{β_1} and k_{β_2} are positive-definite control gains. The new variables, υ_1 and υ_2, are the virtual control inputs to (45) and (46). The control functions, r_{θ_f} and r_{ϕ_f}, are the real control inputs to (45) and (46).

Note that when υ_1 and υ_2 are both equal to zero, (45) and (46) become the exponentially stable subsystems

$$\begin{bmatrix} \dot{\beta}_1 \\ \dot{\beta}_3 \end{bmatrix} = A_{\beta_1}\begin{bmatrix} \beta_1 \\ \beta_3 \end{bmatrix}, A_{\beta_1} = \begin{bmatrix} 0 & 1 \\ -k_{\beta_1}^2 & -2k_{\beta_1} \end{bmatrix}, \tag{52}$$

$$\begin{bmatrix} \dot{\beta}_2 \\ \dot{\beta}_4 \end{bmatrix} = A_{\beta_3}\begin{bmatrix} \beta_2 \\ \beta_4 \end{bmatrix}, A_{\beta_3} = \begin{bmatrix} 0 & 1 \\ -k_{\beta_2}^2 & -2k_{\beta_2} \end{bmatrix}. \tag{53}$$

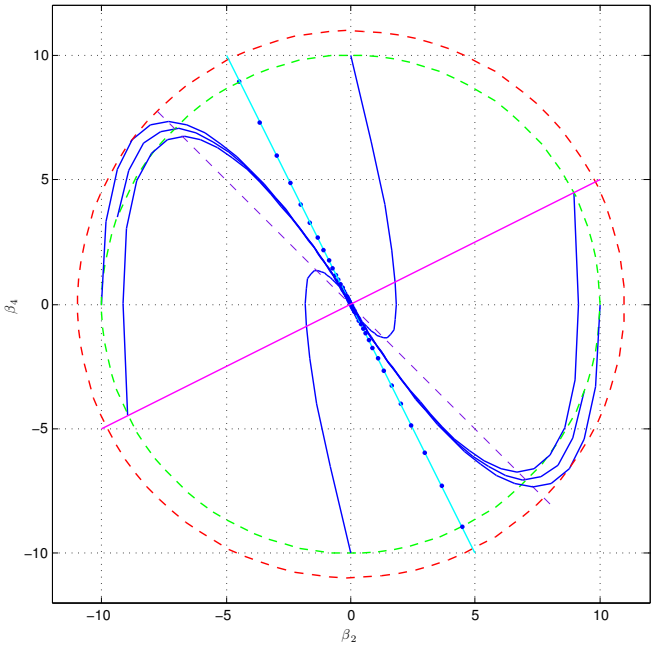

Figure 3. Phase portrait of the unforced response of the abridged model (53) for various initial conditions and control gain $k_{\beta_2} = 2$. Notice the two regions subtended by rotating the line $\beta_4 = -k_{\beta_2}\beta_2$ (cyan) clockwise toward the line $\beta_4 = k_{\beta_2}^{-1}\beta_2$ (magenta). Trajectories originating in these regions will remain in the ball R_δ (green) while exhibiting some overshoot before converging to zero. Also notice the two regions subtended by rotating the line $\beta_4 = k_{\beta_2}^{-1}\beta_2$ (magenta) clockwise toward the line $\beta_4 = -k_{\beta_2}\beta_2$ (cyan). Trajectories originating in these regions will escape the ball R_δ but remain in the larger ball R_ϵ before converging to the origin with no overshoot. As $t \to \infty$, all trajectories tend to the line $\beta_4 = -k_{\beta_2}\beta_2$. Trajectories starting on $\beta_4 = -k_{\beta_2}\beta_2$ will remain thereon while proceeding directly to the origin (dotted traces). The time $t = \tau_{\dot{\beta}_4}$ occurs at the supremum (vertical crest or trough) of $\beta_4(t)$ where each trace intersects the (purple dashed) line $\beta_4 = -\frac{1}{2}k_{\beta_2}\beta_2$ (i.e. $\dot{\beta}_4 = 0$).

In order to drive υ to zero, we set

$$\mu_1 \triangleq -2k_{\upsilon_1}\upsilon_3 - k_{\upsilon_1}^2\upsilon_1, \tag{54}$$

$$\mu_2 \triangleq -2k_{\upsilon_2}\upsilon_4 - k_{\upsilon_2}^2\upsilon_2, \tag{55}$$

where k_{υ_1} and k_{υ_2} are the positive-definite control gains. Substituting (54) and (55) into (45) and (46), we find the globally, exponentially stable subsystem

$$\begin{bmatrix} \dot{\upsilon}_1 \\ \dot{\upsilon}_3 \end{bmatrix} = A_{\upsilon_1}\begin{bmatrix} \upsilon_1 \\ \upsilon_3 \end{bmatrix}, A_{\upsilon_1} = \begin{bmatrix} 0 & 1 \\ -k_{\upsilon_1}^2 & -2k_{\upsilon_1} \end{bmatrix},$$
$$\begin{bmatrix} \dot{\upsilon}_2 \\ \dot{\upsilon}_4 \end{bmatrix} = A_{\upsilon_2}\begin{bmatrix} \upsilon_2 \\ \upsilon_4 \end{bmatrix}, A_{\upsilon_2} = \begin{bmatrix} 0 & 1 \\ -k_{\upsilon_2}^2 & -2k_{\upsilon_2} \end{bmatrix}. \tag{56}$$

Having demonstrated that the unforced β subsystems, (52) and (53), are globally exponentially stable, and taking into account that $r_z + g$ is bounded, we can prove that the cascade β-υ system, (45)-(46), is globally asymptotically stable by showing that the forced β subsystems are input-to-state stable (ISS). Examining the subsystem

$$\begin{bmatrix} \dot{\beta}_2 \\ \dot{\beta}_4 \end{bmatrix} = \begin{bmatrix} \beta_4 \\ (r_z + g)\upsilon_2 - 2k_{\beta_2}\beta_4 - k_{\beta_2}^2\beta_2 \end{bmatrix}, \tag{57}$$

$$\begin{bmatrix} \dot{\upsilon}_2 \\ \dot{\upsilon}_4 \end{bmatrix} = \begin{bmatrix} \upsilon_4 \\ -2k_{\upsilon_2}\upsilon_4 - k_{\upsilon_2}^2\upsilon_2 \end{bmatrix}, \tag{58}$$

we proceed with the ISS-Lyapunov function

$$V = \frac{1}{2}\beta_{24}^T P \beta_{24},\ \beta_{24} \triangleq \begin{bmatrix} \beta_2 & \beta_4 \end{bmatrix}^T, \tag{59}$$

$$P = \begin{bmatrix} 2k_{\beta_2} + k_{\beta_2}^2 k_f & 1 \\ 1 & k_f \end{bmatrix},\ k_f \triangleq \frac{k_{\beta_2}^2 + 1}{2k_{\beta_2}} \geq 1\ \forall k_{\beta_2}, \tag{60}$$

$$V = \frac{1}{2}\left(2k_{\beta_2} + k_{\beta_2}^2 k_f\right)\beta_2^2 + \frac{1}{2}k_f\beta_4^2 + \beta_2\beta_4, \tag{61}$$

$$a_1 \leq V \leq a_2, \tag{62}$$

$$a_1 = \lambda_{min}(P)||\beta_{24}||^2,\ a_2 = \lambda_{max}(P)||\beta_{24}||^2, \tag{63}$$

where λ_{min} and λ_{max} are the minimum and maximum eigenvalues. Taking the derivative of V, we have

$$\dot{V} = \left(2k_{\beta_2} + k_{\beta_2}^2 k_f\right)\beta_2\beta_4 + k_f\beta_4\dot{\beta}_4 + \beta_4^2 + \beta_2\dot{\beta}_4, \tag{64}$$

$$\dot{V} = -k_{\beta_2}^2\left(\beta_2^2 + \beta_4^2\right) + \left(\beta_2 + k_f\beta_4\right)(r_z + g)\,\upsilon_2. \tag{65}$$

Making use of the triangle inequality, we assert

$$\dot{V} \leq -k_{\beta_2}^2(\beta_2^2 + \beta_4^2) + k_f(|\beta_2| + |\beta_4|)|r_z + g||\upsilon_2|, \tag{66}$$

$$\dot{V} \leq -k_{\beta_2}^2(\beta_2^2 + \beta_4^2) + k_f(|\beta_{24}| + |\beta_{24}|)|r_z + g||\upsilon_2|, \tag{67}$$

$$\dot{V} \leq -k_{\beta_2}^2||\beta_{24}||^2 + 2k_f||\beta_{24}|||r_z + g||\upsilon_2|. \tag{68}$$

We can use the term $-k_{\beta_2}^2||\beta_{24}||^2$ to dominate the term $2k_f||\beta_{24}|||r_z + g||\upsilon_2|$ by rewriting (68) as

$$\begin{aligned}\dot{V} \leq & -(1-\zeta)k_{\beta_2}^2||\beta_{24}||^2 - \zeta k_{\beta_2}^2||\beta_{24}||^2 + \\ & + 2k_f||\beta_{24}||\max|r_z + g||\upsilon_2|,\end{aligned} \tag{69}$$

where $0 < \zeta < 1$. We can then say

$$\dot{V} \leq -W_3(\beta_{24})\ \forall ||\beta_{24}||_2 \geq \rho(|\upsilon_2|) > 0, \tag{70}$$

$$W_3(\beta_{24}) = (1-\zeta)k_{\beta_2}^2||\beta_{24}||^2, \tag{71}$$

$$\rho(\upsilon_2) = \frac{k_{\beta_2}^2 + 1}{\zeta k_{\beta_2}^3}\max|r_z + g||\upsilon_2|, \tag{72}$$

with ultimate bound $\sigma = a_1^{-1}(a_2(\rho))$. The foregoing Lyapunov analysis proves that the β subsystems are in fact ISS. We therefore conclude that the closed loop β-υ system is asymptotically stable (in the region where the Euler angles are valid) [8, Theorem 4.19].

In summary, our seven outputs, x_e, y_e, z_e, ψ_{f_e}, ψ_{s_e}, θ_{s_e}, and ϕ_{s_e}, are stabilized using five linear control laws, (36), (37), (28), (29), and (30), and two nonlinear control laws

$$\begin{aligned} r_{\theta_f} \triangleq\ & \cos^2\delta_1\cos\delta_2\left(-2k_{\upsilon_1}\upsilon_3 - k_{\upsilon_1}^2\upsilon_1\right) - 2\tan\delta_1 \\ & - \sec\delta_2(r_{\phi_f}\cos\delta_1\sin\delta_1\sin\delta_2 + 2\delta_3\delta_4\sin\delta_2) \\ & - 2\delta_4^2\cos\delta_1\sin\delta_1\sec^2\delta_2 + \cos\delta_1\sin\delta_1\delta_4^2\delta_3^2 \\ & + \cos^2\delta_1\cos\delta_2\frac{d^2}{dt^2}\left(\frac{2k_{\beta_1}\beta_3 + k_{\beta_1}^2\beta_1 - \ddot{x}_D(t)}{r_z + g}\right), \end{aligned} \tag{73}$$

$$\begin{aligned} r_{\phi_f} \triangleq\ & \cos^2\delta_2\left(-2k_{\upsilon_2}\upsilon_4 - k_{\upsilon_2}^2\upsilon_2\right) - 2\delta_4^2\tan\delta_2 \\ & + \cos^2\delta_2\frac{d^2}{dt^2}\left(\frac{-2k_{\beta_2}\beta_4 - k_{\beta_2}^2\beta_2 + \ddot{y}_D(t)}{r_z + g}\right), \end{aligned} \tag{74}$$

where (73) and (74) are found by inverting (54) and (55).

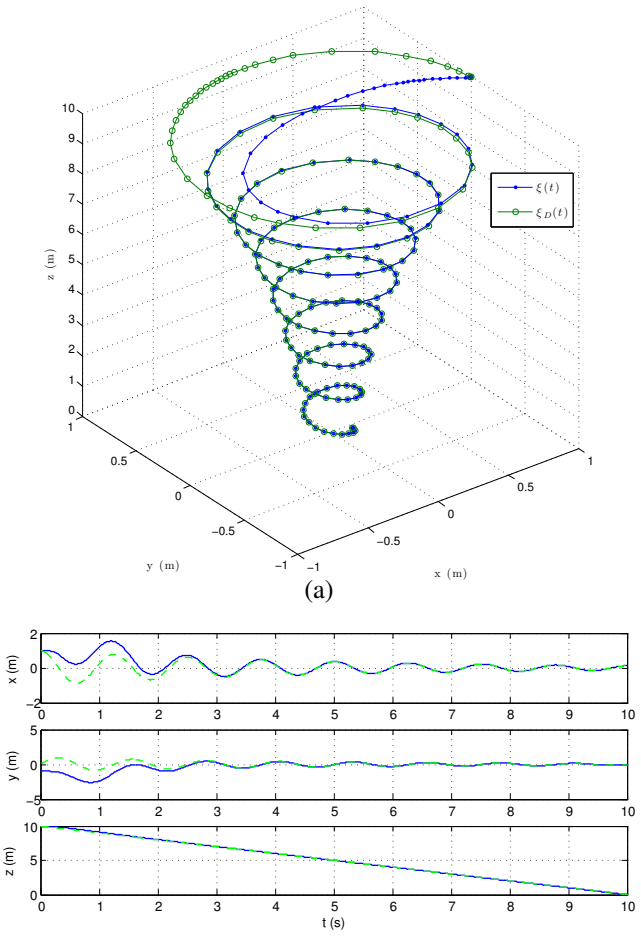

(a)

(b)

Figure 4. Sub-figures (a) and (b) give alternate views of the system's performance while tracking a reference signal (green dashed traces) of the form $x_D(t) = \exp(-t)\cos(t)$, $y_D(t) = \exp(-t)\sin(t)$, $z_D(t) = -t$.

IV. Simulation

Model simulations are carried out in Simulink. Fig. 3 shows a phase portrait of the unforced subsystem (53), for various initial conditions. Fig. 4 shows the full closed-loop system tracking an aggressive 3D position trajectory with zero overshoot. The corresponding control function inputs are plotted in Fig. 5. Lastly, Fig. 6 shows how the control functions are used to steer the flight deck attitude states while the sensor deck attitude states are independently stabilized.

V. Conclusions

The findings of this paper suggest that the proposed control strategy will be suitable for tracking aggressive trajectories in both the position and attitude states of the dual-quad prototype pictured in Fig. 7. The presence of significant unmodeled dynamics could, however, render the obtained results invalid. Unmodeled dynamics are most likely to result from unintended coupling between the sensor and flight decks. To address this concern, the geometry of the design is such that aerodynamic interference between the decks is minimal. Similarly, mechanical interference between the decks is made negligible by virtue of a low-friction ball joint.

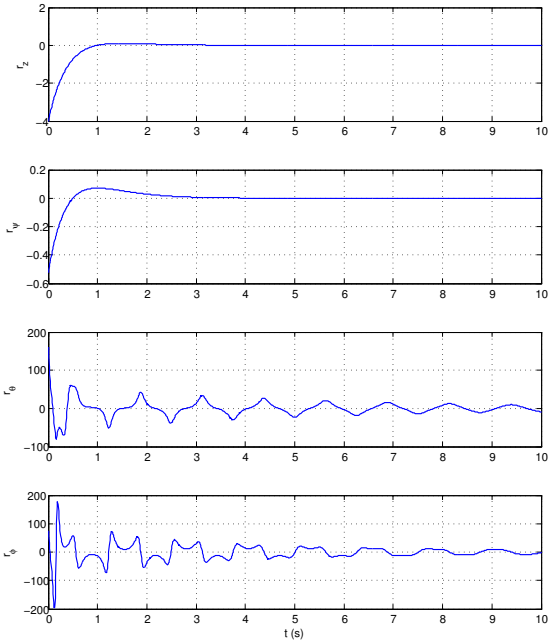

Figure 5. The top two subplots show linear trajectory tracking in the altitude and flight deck yaw inputs, while the bottom two subplots show nonlinear trajectory tracking in the flight deck pitch and roll inputs.

The decision to actuate the sensor deck with propellers was not made trivially. While a servo assembly would have been simpler to implement, adding servos would increase the vehicle's overall weight without also increasing the thrust available to lift said weight. A nested quadrotor, on the other hand, offers attitude control as well as increased thrust. Additionally, the inclusion of servos would introduce new dynamics to the system while the inclusion of a second quadrotor merely duplicates the existing dynamics.

Perhaps the greatest motivation for choosing the nested quadrotor design is the ability to apply a tugboat concept where a larger vessel outsources certain motion control tasks to a smaller vessel. In [9], we find a framework for robust perching and landing, while in [10], we find a framework for aerial grasping and lifting. Together, these suggest that it is feasible to use a quadrotor MAV to tow a larger quadrotor UAV. In this case, the larger UAV would serve as the sensor deck, using large-diameter propellers to carry the vision system payload more efficiently. In order to allow the UAV sensor deck to maintain its motion constraint while carrying out the vision tracking task for an MAV swarm, one of the MAVs would dock with and tow the UAV as needed. As such, the dual-quad prototype is a physical model of the docking maneuver between two rotorcraft in a heterogeneous swarm.

References

[1] A. Kushleyev, D. Mellinger, and V. Kumar, "Towards a swarm of agile micro quadrotors," *Robotics: Science and Systems*, July 2012.

[2] A. Haque and J. D. Dickman, "Vestibular gaze stabilization: different behavioral strategies for arboreal and terrestrial avians," *J. Neurophysiology*, vol. 93, no. 3, pp. 1165–1173, 2005.

[3] T. Madani and A. Benallegue, "Control of a quadrotor mini-helicopter via full state backstepping technique," in *Decision and Control, 2006 45th IEEE Conference on*, dec. 2006, pp. 1515 –1520.

[4] P. Castillo, R. Lozano, and A. Dzul, "Stabilization of a mini rotorcraft with four rotors," *Control Systems, IEEE*, vol. 25, no. 6, pp. 45 – 55, dec 2005.

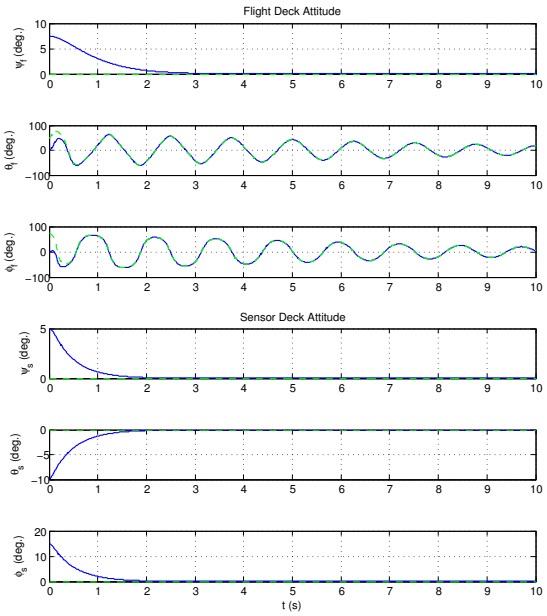

Figure 6. The top three subplots show the flight deck tracking a periodic trajectory (green dashed traces) while the bottom three subplots show the sensor deck independently stabilized at the origin.

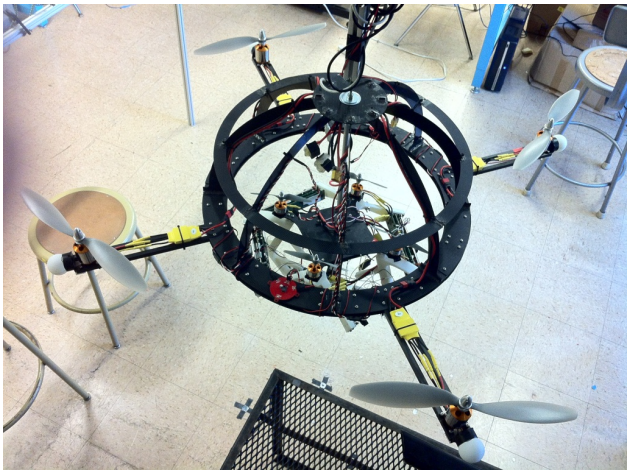

Figure 7. A small inner quadrotor (sensor deck) carrying a vision system, is pictured nesting inside a large outer quadrotor (flight deck).

[5] S. Seghour, M. Bouchoucha, and H. Osmani, "From integral backstepping to integral sliding mode attitude stabilization of a quadrotor system: Real time implementation on an embedded control system based on a dspic c," Istanbul, Turkey, 2011, pp. 154 – 161. [Online]. Available: http://dx.doi.org/10.1109/ICMECH.2011.5971273

[6] G. Raffo, M. Ortega, and F. Rubio, "Backstepping/nonlinear h-infinity control for path tracking of a quadrotor unmanned aerial vehicle," in *American Control Conference, 2008*, june 2008, pp. 3356 –3361.

[7] A. Das, F. Lewis, and K. Subbarao, "Backstepping approach for controlling a quadrotor using lagrange form dynamics," *Journal of Intelligent and Robotic Systems: Theory and Applications*, vol. 56, no. 1-2, pp. 127 – 151, 2009. [Online]. Available: http://dx.doi.org/10.1007/s10846-009-9331-0

[8] H. Khalil, *Nonlinear Systems*. Prentice Hall, Jan. 2002. [Online]. Available: http://www.worldcat.org/isbn/0131227408

[9] D. Mellinger, M. Shomin, and V. Kumar, "Control of quadrotors for robust perching and landing," in *Proceedings of the International Powered Lift Conference*, Oct 2010.

[10] D. Mellinger, Q. Lindsey, M. Shomin, and V. Kumar, "Design, modeling, estimation and control for aerial grasping and manipulation," in *Proceedings of the IEEE International Conference on Intelligent Robots and Systems (IROS)*, Sept 2011.